Correlated heterogeneous deformation of entangled fiber networks

R. C. Picu[1,2] and G. Subramanian[2]

[1]*Department of Mechanical, Aerospace and Nuclear Engineering, Rensselaer Polytechnic Institute, Troy, New York 12180, USA*

[2]*Scientific Computations Research Center, Rensselaer Polytechnic Institute, Troy, New York 12180, USA*

(Received 9 March 2011; published 2 September 2011)

We study the deformation of a network of entangled non-cross-linked semiflexible fibers subjected to compression. We show that the deformation is intermittent, heterogeneous, and dominated by the occurrence of avalanches. Avalanches imply relative fiber sliding and rearrangement and lead to a serrated stress-strain curve. A large fraction of the fibers in the system contribute to an avalanche, and the amplitudes of the sliding events are correlated spatially. This phenomenon is qualitatively similar in systems with and without friction between fibers and is not due to frictional stick slip.

DOI: 10.1103/PhysRevE.84.031904 PACS number(s): 87.16.Ka, 83.80.Kn

I. INTRODUCTION

Systems composed of entangled fibers are central to a large number of materials, both biological and man-made. One of the most important biological applications is the cytoskeleton of eukaryotic cells, which is composed of a complex protein fiber network [1]. The F-actin filaments of the cytoskeleton are semiflexible, i.e., their persistence length is larger than the mean segment length of the network (segment between cross-links). Another important biological example is connective tissue whose mechanical properties are determined by collagen fiber networks [2].

Fiber networks are the essential component of many man-made materials. At present, composites made from entangled carbon nanotubes are intensely studied [3], while entangled fibers are used in many consumer products, such as wipes, baby diapers, and clothing, having insulation, filtration, and fluid absorption functions. Paper is one of the oldest man-made materials based on semiflexible random fiber networks. In all these systems and in view of the structural function of the network, mechanics is important. In some applications, a theoretical understanding, leading to modeling the mechanics of fiber systems, is desirable. For example, modeling the mechanics of the cytoskeleton is necessary in order to make progress toward understanding cellular biochemical processes.

In mechanics, the classical view is that the deformation of materials is a homogeneous process. Localization of deformation in narrow regions, e.g., shear bands, is treated as a separate phenomenon, more or less on the fringes of continuum theories, very much like fracture. However, evidence is being accumulated that the physics of deformation is different. An example is provided by plastic deformation of crystalline solids mediated by dislocations, which has been viewed as a homogeneous flow. A fundamentally different picture emerged during the past several years [4], that of a complex intermittent phenomenon characterized by dislocation avalanches [5], time correlations [6], and fractal patterns [7]. A similar view is developing for the deformation of granular materials, which is characterized by avalanches and intermittency [8].

In this paper, we show that the deformation of random semiflexible non-cross-linked fiber systems is also heterogeneous and highly nonaffine with avalanches associated with the relative sliding of fibers and fiber rearrangements.

II. MODEL

Here, semiflexible cylindrical fibers are modeled with the bead-spring model frequently used in polymer physics [9]. Each fiber is represented by a chain of beads connected by harmonic springs. The energy associated with the axial and bending deformations of the fiber are given by $U_a = k_a(r - r_0)^2/2$ and $U_b = k_b(\theta - \theta_0)^2/2$, respectively, where r and r_0 are the current and the reference distances between successive beads and θ and θ_0 are the current and reference angles made by successive bonds along the fiber. A shifted Lennard-Jones (LJ) potential is used for nonbonded interactions $U_c = 4\varepsilon[(s/r)^{12} - (s/r)^6] + \varepsilon$ for $r < r_0$ and $U_c = 0$ for $r > r_0$. The potential is truncated at its minimum $r_0 = 2^{1/6}s$ to eliminate the cohesive effect, and $\theta_0 = \pi$, i.e., fibers are straight when unloaded. s and e become the units of length and energy of the problem, respectively. The axial stiffness of the fiber is in the units of this model $EA = k_a r_0$, while the bending stiffness is $EI = k_b r_0$. E represented the Young's modulus of the fiber material, while A and I are the cross-section area and the moment of inertia of the fiber, respectively. The equivalence between the bead-spring model quantities and the parameters describing the elasticity of a cylindrical fiber is established via the contact between fibers. The elastic contact between two cylinders of the same radius is described by Hertz's formula [10]. Requiring that the contact energy computed with this continuum model equals the energy of nonbonded interactions evaluated with the LJ potential at same relative bead displacement (interpenetration of fibers) leads to a relationship between the reduced Young's modulus of the fiber $E/(1-\nu^2)$ (ν is Poisson's ratio) and the energyconstant e : $E/(1-\nu^2) \sim 420.4e/s^3$. Furthermore, approximating $1 - \nu^2 = 1$, one obtains, for the two constants entering U_a and U_b, $k_a = 372.2\varepsilon/s^2$ and $k_b = 29.3\varepsilon$. The ratio of the bending to axial stiffness is $l_b = \sqrt{EI/EA} = 0.28s$. These considerations allow mapping the discrete model of a fiber to a continuous cylindrical Euler-Bernoulli beam of diameter r_0 [11]. Furthermore, the axial stiffness is large enough for fibers not to cross each other. It was tested (by increasing the bead number density along each fiber) that the roughness due to the discrete representation used for fibers does not lead to artificial friction or adhesion of fibers in contact [11].

Initial configurations are obtained by growing straight fibers with random orientations in a large simulation box with periodic boundary conditions. At this stage, the density $\rho = NL_0A/L^3$ is low to minimize fiber interaction. N represents the total number of fibers in the model, $A = \pi r_0^2/4$ is the area of the fiber section, L_0 is the fiber length, and L is the size of the simulation box. Here, $N = 1200$, $L_0 = 50s$, and the size of the model when fibers are generated is $L = 509.7s$. The resulting configuration is subjected to stepwise hydrostatic compression. In order to avoid artifacts introduced by the periodic boundary conditions, the size of the simulation box at the maximum density is kept larger than L_0.

The system is loaded by imposing displacements along the model boundaries; the fibers move as in molecular dynamics. The equations of motion include a small damping term, which cools down the system toward the zero Kelvin equilibrium state. Coulomb friction between fibers may be included [11], however, the results reported here correspond to a vanishing friction coefficient $\mu = 0$. The deformation is imposed in small steps, and the system is allowed to reach its static equilibrium state after each step. The sequence of these equilibrium configurations is considered the quasistatic athermal trajectory of the system.

The deformation is described by a spherical deformation gradient tensor $\mathbf{F} = q\mathbf{I}$, where $\mathbf{I}$ is the identity matrix and q is a variable parameter, and the resulting dilatation strain Δ, which is the trace of the Green strain $\mathbf{E}$, is $\Delta = (3/2)(q^2 - 1)$. Parameter q is related to the density as $q = (\rho_0/\rho)^{1/3}$, with ρ and ρ_0 being the current and reference densities ($\rho_0 = 1$). The Cauchy stress is evaluated as $\boldsymbol{T} = \frac{1}{\det F}\boldsymbol{F}\frac{d\hat{U}}{d\boldsymbol{E}}\boldsymbol{F}^T$, with $\hat{U}$ being the strain energy density that is computed by summing up contributions of bending $\hat{U}_b$, axial $\hat{U}_a$, and contact $\hat{U}_c$ energies over all interactions. $\mathbf{T}$ results in a spherical tensor with diagonal components given by $\sigma = -3\frac{\rho^2}{\rho_0}\frac{d\hat{U}}{d\rho}$. Note that σ is equal to the pressure.

During deformation, contacts are created between fibers. The plane of a contact is the common tangent plane of the two beads forming the contact. The sliding distance in the given load increment in each contact S is defined as the norm of the component of the vector of the relative displacement projected in the plane of the contact. The mean sliding distance $\bar{S}$ is computed as the average over the entire population of contacts in the current state.

III. RESULTS

As the network is compacted from the sparse state in which fibers are created, it reaches geometric and then stiffness percolation. These thresholds have been discussed in the literature [12–14]. At higher densities, each fiber makes multiple contacts, which define fiber segments. The distribution function of segment lengths is Poisson [15]. The mean segment length l_c decreases as the density increases as $l_c \sim 1/\rho$ [15].

Figure 1 shows the variation of the stress σ with the dilatation strain during compaction (red, continuous line). The inset shows the same quantity in log-log coordinates and for a broader range of the variable. Stiffness percolation takes place at $\Delta \approx 25$ (vertical line in the inset). The stress-dilatation

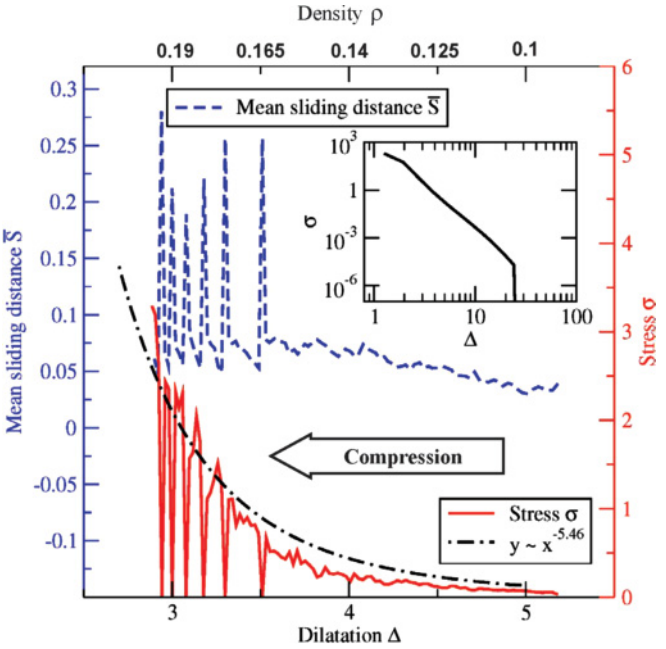

FIG. 1. (Color online) Variation of the hydrostatic stress σ (continuous red line and right vertical axis) and of the mean sliding measure $\bar{S}$ (dashed blue line and left vertical axis) with the dilatation strain Δ (or density, top axis). The units for σ and $\bar{S}$ are e/s^3 and s, respectively. The inset shows the stress-strain curve in log-log coordinates evidencing the power law dependence of stress on strain. The dashed-dotted black line in the main figure shows the fit $\sigma \sim \Delta^{-5.46}$ to the curve in the inset. Serrations in the stress-strain curve and the spikes in the $\bar{S}$ function are correlated.

curve is approximated by the power function $\sigma \sim \Delta^{-5.46}$, which, for this range of densities, is equivalent to $\sigma \sim \rho^{4.1}$. The power law variation of the stress with the density was confirmed experimentally [16,17] and numerically [14,18] and was predicted theoretically based on mean field considerations [19,20]. The value of the exponent depends on the nature of the system, testing conditions, and likely on l_b and ranges from approximately 2 to 6 [16–18]. The models available [19,20] predict an exponent of 3. The bulk modulus also scales in our model as $K \sim \rho^{4.75}$, while the experimental modulus scales as $K \sim \rho^m$, where m increases from 3 to 5 as the sample mass increases. The model predicts that interfiber friction has no effect on the respective power law functions and exponents [11] in agreement with the experiments. The curve in the main figure exhibits large serrations once Δ decreases below 3.5. These are not visible in the curve in the inset since those data are collected less frequently.

The variation of the mean sliding $\bar{S}$ is also shown in Fig. 1 (blue, dashed line). The striking feature of the plot is the strong correlation observed between spikes in $\bar{S}$ and the sharp drops in the stress. This indicates that avalanches form as the system is compressed, and hence, deformation is intermittent. Avalanches are not observed when the density is small. For $\Delta > 3.5$, $\bar{S}$ is approximately constant. Likewise, $\bar{S}$ in load increments between avalanches and for $2 < \Delta < 3.5$ is almost independent of Δ.

This behavior is observed in earthquake mechanics where many small tremors occur between large earthquakes. In

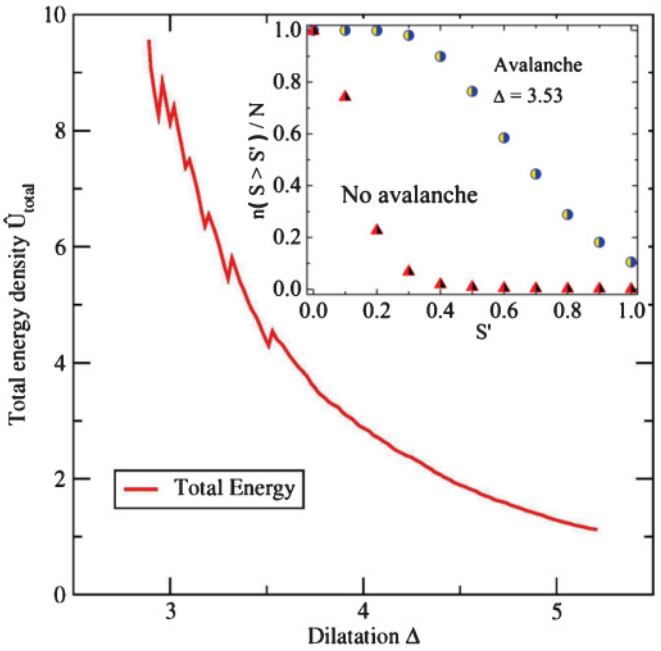

FIG. 2. (Color online) Variation of the total strain energy density $\hat{U}$ with the strain Δ. Serrations are observed in the energy curve. The inset shows the fraction of chains having at least a contact that slides more than S', $n(S > S')/N$, versus S', for two load steps with and without avalanches.

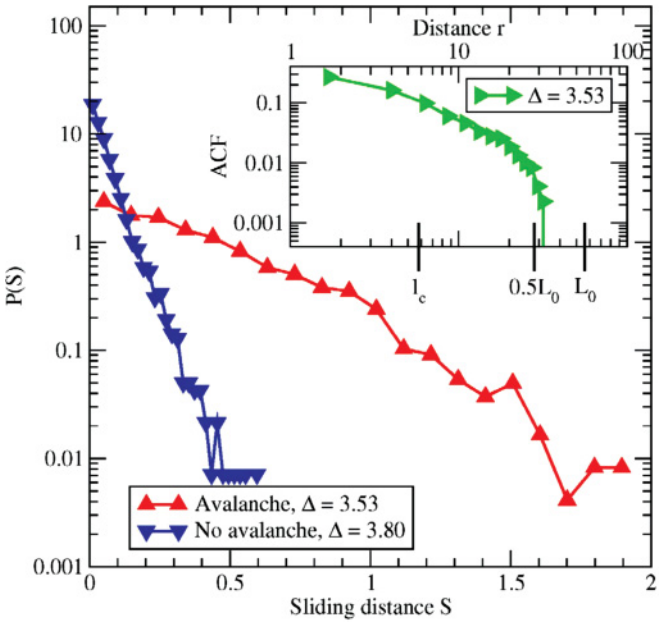

FIG. 3. (Color online) PDF of the sliding distance S in a load step in which an avalanche is observed (triangles and red curve) and in a load step in which there is no avalanche (reversed triangles and blue curve). Both PDFs are exponential. The inset shows the autocorrelation function of S evaluated during an avalanche. The mean segment length l_c and the fiber length L_0 are also indicated.

metals, although the macroscopic deformation seems homogeneous, on the mesoscale, one observes avalanches and intermittent dynamics [7]. Similar observations were made in metallic micro- and nanopillars subjected to compression [21]. In solid solutions, heterogeneous plasticity is observed at the macroscopic scale [22]. Sliding of two elastic bodies in contact takes place by stick slip, which is another example of intermittent dynamics.

The variation of the total strain energy density $\hat{U}$ with Δ is shown in Fig. 2. The function is smooth for $\Delta > 3.5$ and exhibits serrations for smaller Δ. The presence of these drops shows that this slowly driven system evolves over a rough energy landscape. The energy is purely elastic, and its dependence on strain is not monotonic even at small deformations since the relative positions of fibers may change.

A large number of fibers is involved in an avalanche. The inset to Fig. 2 shows the fraction of all fibers in the system containing at least a contact that slides more than $S = S'$, $n(S > S')/N$, versus S'. The two curves correspond to the load step at $\Delta = 3.53$, when an avalanche is seen, and to the immediately following load step in which there is no avalanche. While in the load step without an avalanche no fiber slides more than $S = 0.4s$, during an avalanche 90% of the fibers slide more than this threshold, and 1/3 of fibers slide even more than $0.8s$.

To gain further insight into the nature of avalanches, we investigated the probability distribution function (PDF) of S, the spatial correlation of S, and the spatial distribution of sliding events during an avalanche. The PDF of sliding amplitudes is shown in Fig. 3. Two curves are presented for a step with and without an avalanche. Both distribution functions are exponential and have different means. Given the nature of this PDF, the mean (curve $\bar{S}$ in Fig. 1) fully characterizes the sliding events in each load step.

One may inquire whether the occurrence of an avalanche may be associated with a particular type of distribution of contact energies in the previous load step. The PDF of contact energies is also exponential, and no difference is seen between states right before and right after an avalanche. The PDF evolves with Δ, but for the small variation in the strain discussed here, PDFs for various load steps are identical within the statistical noise. This observation differs from the discussion in Ref. [23] where it was concluded that contact energies are power law distributed over a broad range of energies. In Ref. [23], the contacts are not allowed to slide and are stabilized by introducing stiff bonds; the strain energy of these cross-linkers is considered contact energy. Our results indicate that a power law distribution of contact energies is not required in order to observe heterogeneous deformation.

The inset to Fig. 3 shows the autocorrelation function (ACF) of S evaluated during the avalanche at $\Delta = 3.53$. The ACF is computed by considering values of S at all contacts in the simulation and by averaging over multiple origins. The sliding events are correlated up to a distance of approximately half of the undeformed fiber length ($L_0/2$). The value of the mean segment length l_c, at the given Δ, is indicated on the horizontal axis for reference. Since many fibers are involved in an avalanche (inset to Fig. 2), the ACF data indicate that the sliding magnitudes of neighboring fibers are not long-range correlated.

This conclusion is supported by the spatial distribution of sliding events. The pair distribution function $g(r)$ of sites where sliding takes place is evaluated. The distinction between contacts that do not slide and those that slide in a given load

step is made using a threshold $S_{th} = 0.5s$. $g_{sl}(r)$, computed based on contacts at which sliding is observed ($S > S_{th}$), shows clustering over a range comparable to $L_0/2$. $g_{all}(r)$, computed based on the location of all contacts (independent of S), shows less clustering and extends over the same range. At small r, $g_{all}(r)$ is controlled by the exponential PDF of segment lengths. Hence, in this limit, the pair distribution function should scale as $g_{all}(r) \sim \exp(-r/l_c)/r^2$. At large r, the function samples a random distribution of points in space. No clustering is obtained if $g(r)$ is computed using the location of the centers of mass of fibers that slide more than S_{th}. These centers are randomly distributed in space. Given the large number of fibers with $S > S_{th}$ (75% of the $N = 1200$ fibers in the model for the load step at $\Delta = 3.53$), this indicates that avalanches do not create a specific structure, rather, the initial random distribution is retained during deformation.

The physical picture, which is emerging, is that an avalanche is produced by a large-scale fiber rearrangement mediated by sliding at most fiber-fiber contacts. The sliding magnitudes are correlated only over a distance equal to half the fiber length since entire fibers move; this rearrangement does not have the structure of a shear-driven localization band.

The effect of interfiber Coulomb friction on the statistics of sliding events was investigated in systems with friction coefficients $\mu = 0.1$ and 1. The method of accounting for friction in this model is discussed in detail in Ref. [11]. In systems with friction, the magnitude of serrations in both $\hat{U}$ and $\bar{S}$ is reduced relative to the $\mu = 0$ case. This indicates that the phenomenology discussed in this paper is not due to frictional stick slip, which is known to lead to intermittent dynamics [24].

IV. CONCLUSION

In conclusion, we have shown that the deformation of a system of non-cross-linked semiflexible fibers subjected to compression is heterogeneous, occurring largely through avalanches associated with fiber rearrangements. The resulting stress-strain curve is serrated in a certain range of densities. These features are commonly observed in random discrete systems, such as granular media and dislocation-mediated crystal plasticity, but have not been evidenced so far in fiber networks.

[1] *Cytoskeletal Mechanics*, edited by M. R. K. Mofrad and R. D. Kamm (Cambridge University Press, Cambridge, UK, 2006).
[2] B. R. Martin, D. B. Burr, and N. A. Sharkey, *Skeletal Tissue Mechanics* (Springer, New York, 2004).
[3] W. Zhang, R. C. Picu, and N. Koratkar, Appl. Phys. Lett. **91**, 193109 (2007).
[4] M. Zaiser, Adv. Phys. **55**, 185 (2006).
[5] M. C. Miguel, A. Vespignani, and S. Zapperi, Nature (London) **410**, 667 (2001).
[6] J. Weiss and M.-C. Miguel, Mater. Sci. Eng. A **387-389**, 292 (2004).
[7] J. Weiss and D. Marsan, Science **299**, 89 (2003).
[8] R. Candelier, O. Dauchot, and G. Brioli, Phys. Rev. Lett. **102**, 088001 (2009).
[9] K. Kremer and G. Grest, J. Chem. Phys. **92**, 5057 (1990).
[10] H. Hertz, J. Reine Angew. Math. **92**, 156 (1881).
[11] G. Subramanian and R. C. Picu, Phys. Rev. E **83**, 056120 (2011).
[12] A. L. R. Bug, S. A. Safran, and I. Webman, Phys. Rev. Lett. **54**, 1412 (1985).
[13] I. Balberg, N. Binenbaum, and N. Wagner, Phys. Rev. Lett. **52**, 1465 (1984).
[14] D. Rodney, M. Fivel, and R. Dendievel, Phys. Rev. Lett. **95**, 108004 (2005).
[15] O. Kallmes and H. Corte, Tappi J. **43**, 737 (1960).
[16] J. Masse, L. Salvo, D. Rodney, Y. Brechet, and O. Bouaziz, Scr. Mater. **54**, 1383 (2006).
[17] D. Poquillon, B. Viguier, and E. Andrieu, J. Mater. Sci. **40**, 5963 (2005).
[18] D. Durville, J. Mater. Sci. **40**, 5941 (2005).
[19] C. M. vanWyk, J. Text. Inst. **37**, T285 (1946).
[20] S. Toll, Polym. Eng. Sci. **38**, 1337 (1998).
[21] M. Zaiser, J. Schwerdtfeger, A. S. Schneider, C. P. Frick, B. G. Clark, P. A. Gruber, and E. Arzt, Philos. Mag. **88**, 3861 (2008).
[22] R. C. Picu, G. Vincze, F. Ozturk, J. J. Gracio, F. Barlat, and A. M. Maniatty, Mater. Sci. Eng. A **390**, 334 (2005).
[23] J. A. Astrom, J. Timonen, M. Myllys, J. Fellman, and J. LeBell, Eur. Phys. J. E **22**, 61 (2007).
[24] T. Baumberger and C. Caroli, Adv. Phys. **55**, 279 (2006).